Design rules for electrode arrangement in an air-breathing alkaline direct methanol laminar flow fuel cell

Michael R. Thorson, Fikile R. Brushett, Chris J. Timberg, Paul J.A. Kenis*

Department of Chemical & Biomolecular Engineering, University of Illinois at Urbana-Champaign, USA

HIGHLIGHTS

► Experimentally investigated the relationship between electrode length and current density for a range of reactant flow rates.
► Highlighted the effect of electrode aspect ratio on performance, specifically current density.
► Systematically investigated how to achieve 75% fuel conversion using minimum number of electrodes and electrode area.
► Analysis can be applied to many other microfluidic electrochemical reactors.

ARTICLE INFO

ABSTRACT

The influence of electrode length on performance is investigated in an air-breathing alkaline direct methanol laminar flow fuel cell (LFFC). Depletion of methanol at the electrode surface along the direction of flow hinders reaction kinetics and consequently also cell performance. Reducing the electrode length can decrease the influence of boundary layer depletion, and thereby, improve both the current and power densities. Here, the effect of boundary layer depletion was found to play a significant effect on performance within the first 18 mm of an electrode length. To further utilize the increased power densities provided by shorter electrode lengths, alternative electrode aspect ratios (electrode length-to-width) and electrode arrangements were explored experimentally. Furthermore, by fitting an empirical model based on experimentally obtained data, we demonstrate that a configuration comprised of a series of short electrodes and operated at low flow rates can achieve higher current and power outputs. The analysis of optimal electrode aspect ratio and electrode arrangements can also be applied to other microfluidic reactor designs in which reaction depletion boundary layers occur due to surface reactions.

© 2012 Elsevier B.V. All rights reserved.

1. Introduction

An ever increasing demand for high power density, portable electronic devices (*e.g.*, smartphones, laptops) with a fast recharge has motivated the development of many micro-scale fuel cells [1–5]. Small-scale fuel cells demonstrate superior energy densities compared to rechargeable batteries; offering smaller, and lighter alternatives for applications requiring portable power sources [6]. Specifically, developments in both novel fuel cell catalysts and electrode assemblies, and advances in fabrication have enabled the miniaturization of fuel cells capable of integration in small portable applications [2–4,7,8]. Furthermore, liquid organic feed sources, such as methanol, have a distinct advantage compared to gaseous hydrogen feed sources as the fuel can be stored safely at low

pressure, in an energy dense form. In comparison to traditional batteries, the liquid nature of methanol also enables nearly instantaneous recharging via refilling or changing-out of a fuel cartridge. Additionally, the use of a membraneless laminar flow fuel cell (LFFC) enables the use of alkaline media, avoiding the membrane-associated issues typically encountered in alkaline fuel cells. Furthermore, in alkaline media, the reaction kinetics are better at both the anode [9] and the cathode [10], and high performance can be achieved with abundant and cheap catalysts such as Ag [11–15].

LFFCs have several further attractive characteristics. The flowing liquid electrolyte stream mitigates water management issues and enables fuel flexibility [16]. Alternative fuel feed mechanisms [17–19], as well as modifications to electrode location and method of catalyst deposition [20–24] have led to improved current densities. Alternative cell designs [25–27] (*e.g.*, F, Y, and T channel geometries) and further modifications to LFFC configurations [28,29] (*e.g.*, herringbone mixers, multiple inlets) have improved

* Corresponding author. Tel.: +1 217 265 0523.
  E-mail addresses: kenis@illinois.edu, kenis@uiuc.edu (P.J.A. Kenis).

both fuel conversion and current density, while helping to mitigate fuel crossover. Recently, nanoporous separators have been employed to minimize the interfacial area between the fuel and electrolyte streams, thereby drastically reducing fuel crossover [30].

A major limitation to obtaining higher current densities in present LFFC configurations is the depletion of fuel along the electrode surface. Several computational studies have reported on this boundary layer depletion issue. Specifically, using a CFD model of the formic acid reaction within a membraneless LFFC, Bazylak et al. showed that a ~15 μm thick boundary layer formed within 1 mm, which drastically increased the mass transport limitations [31]. Yoon et al. modeled a similar scenario to examine the electrode performance for formic acid oxidation with a membraneless LFFC [28] in which they showed that depletion quickly becomes a major limitation within the fast forming boundary layer and that the current density will decrease by a factor of 4 within the first centimeter of the electrode length. Additionally, Khabbazi et al. modeled the influence of electrode length (8–30 mm) on electrode performance and showed that the power density could be increased by ~80% by reducing the electrode length [32]. These aforementioned models all assume well developed flow profiles with smooth electrodes. Actual electrode surfaces will have inherent roughness, which will influence the diffusion of fuel to reactive sites on the electrode. Moreover, the local geometries and the orientation of the inlets for the electrolyte and fuel streams will affect the formation of the boundary layer on the fuel stream and thereby, change the influence of electrode length on performance.

Here, we experimentally studied the influence of electrode length on performance in an air-breathing alkaline direct methanol LFFC with the aim of formulating design rules for multichannel LFFCs with optimum specific energy. The effects of aspect ratio (length-to-width) on electrode performance, and thus overall fuel cell performance, was investigated. Furthermore, similar experiments were used to develop an empirical model, which predicts the optimal electrode configurations for a multichannel LFFC.

2. Experimental

2.1. Fuel cell assembly

Fig. 1 shows the LFFC used in this study, a configuration similar to those we previously reported [30,33]. Instead of graphite, we
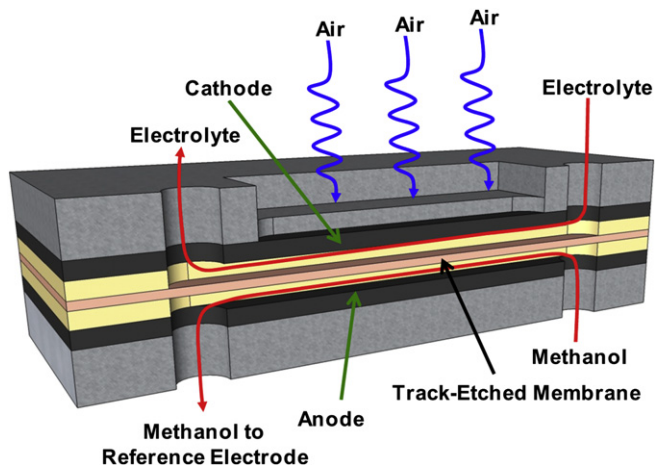

Fig. 1. Schematic of an alkaline, air-breathing, direct methanol, laminar flow fuel cell (LFFC). Two 1-mm thick PMMA windows provide the flow fields for the electrolyte and fuel streams between the current collectors and the nanoporous separator.

used two stainless steel backing plates (6×3 cm^2) as current collectors. We chose to use stainless steel plates backing plates to improve the structural strength (prevent cracking of the graphite), reduce contact resistance between the wires from the potentiostat and the backing plate, and improve the pressure distribution of the bolts. In agreement with prior work [34], we did not observe corrosion of the steel backing plates of our setup. Wires with banana clips plugged directly into precision-machined 3/16″ holes in the anode and cathode current collectors connected the cell with an in-house built load box. The cathode current collector had a precision-machined 3-mm wide by 40-mm long window that enabled diffusion of oxygen from air to the cathode for an air-breathing configuration. Two 1-mm thick poly(methyl methacrylate) (PMMA) sheets with precision-machined 3-mm wide by 50-mm long windows served as the channels for the electrolyte flow field within the fuel cell. We used Teflon sheets with precision cut windows (3-mm wide and 2.25, 4.5, 9, 18, or 36-mm long), placed between the electrode and the flow channel, to vary the area of the cathode and anode exposed to air and fuel, respectively. A polycarbonate track-etch membrane (6-μm thick, 0.05-μm pore size, PCT0059030 Sterlitech Corporation) was placed between the two PMMA flow channels to reduce the liquid–liquid interfacial area thereby reducing the effects of fuel crossover [30]. The cell was held together by four insulated bolts (McMaster Carr).

2.2. Electrode preparation

The anode was prepared via painting a 1:1 (V/V) H$_2$O:2-propanol solution containing dispersed catalyst onto the hydrophobized side of a sheet of Toray carbon paper (TGP-H-120, Fuel Cell Earth) such that the final catalyst loading was 2 mg cm^{-2} of unsupported Pt/Ru alloy catalyst (50:50 wt%, Alfa Aesar) and 0.1 mg cm^{-2} of Nafion binder (LIQUION LG-1105, Ion Power). Similarly, the cathode was prepared via painting a catalyst solution on Toray carbon paper resulting in a catalyst loading of 2 mg cm^{-2} of Pt/C catalyst (50% mass on Vulcan carbon, E-Tek) and 0.1 mg cm^{-2} of Nafion binder. More details on this catalyst deposition procedure have been reported previously [35].

2.3. Fuel cell testing

The fuel cell assembly was tested under alkaline conditions using an anolyte comprised of fuel + 1 M potassium hydroxide (KOH, Sigma Aldrich), and a catholyte comprised of 1 M KOH. The KOH electrolyte solutions are not expected to damage the gas diffusion electrodes via carbonate poisoning because the application of a flowing electrolyte removes carbonates from the electrolyte system [36].

Four methanol (Sigma Aldrich) concentrations (0.375, 0.75, 1.5, and 3.0 M) were used in the anolyte. The flow rates of the fuel and electrolyte streams within the fuel cell were regulated with a syringe pump (Harvard Instruments PHD 2200). After flowing through the reactor, the electrolyte stream exited the fuel cell through a plastic tube (Cole Palmer, i.d.=1.57 mm) and was collected in a glass beaker. As shown in previous work, no significant potential drop occurs between the fuel cell and the collection beaker [37]. Individual electrode potentials were measured using multimeters (Fluke 8 III) relative to an Ag/AgCl reference electrode (saturated NaCl, BAS, West Lafayette, IN) in the collection beaker for the fuel stream. Fuel cell measurements were conducted at 0.05 V intervals using an in-house built load box. The current was measured once steady-state had been reached for a given potential, which typically took between 3 and 5 min. The geometric surface areas used to calculate the reported current and power densities were equal to the exposed electrode areas (0.0625, 0.125, 0.25, 0.5,

and 1 cm^2 for the 3-mm wide and 2.25, 4.5, 9, 18, 36-mm long Teflon windows). All conversions are calculated based on the current recorded by the potentiostat, and consequently, do not include Faradaic losses due to fuel crossover in the conversion calculation.

2.4. Modeling

Based on the fuel conversion in the presence of various length electrodes in a single LFFC unit, we modeled the anticipated conversion for a fuel cell stack comprised of a series of electrodes. Several assumptions went into the development of this model. First, performance losses associated with fuel crossover were not take into account because the use of a separator drastically reduces the crossover effect as we previously reported [30]. Second, we assumed that, for the conditions tested, the current density of the fuel cell can be interpolated in a linear fashion relative to the inlet fuel concentration (see Supplementary information). Third, we assumed that fuel streams between consecutive cells had the opportunity to restore any concentration depletion layers generated on the electrodes in the previous cell. In other words, a well-mixed fuel stream, but of lower fuel concentration, will enter each successive cell.

For this model, a full factorial experimental design was developed in which we varied the methanol concentration of the fuel stream (0.75, 1.5, and 3.0 M), the flow rates of the methanol and electrolyte streams (0.1, 0.2, 0.4, and 0.8 ml min^{-1}), and the length of the exposed electrode (9, 18, and 36 mm). In each experiment, the KOH concentration in the electrolyte and fuel streams was 1 M. For each condition, a polarization curve was obtained to identify a power output for a given current density. For each electrode length and flow rate tested, the measured current was plotted as a function of the three methanol concentration. Then, after interpolation over the regions 0.75–1.5 M and 1.5–3.0 M, the slope m of these interpolated lines is calculated using the following equation:

$$m = \frac{i_{high} - i_{low}}{C_{high} - C_{low}} \tag{1}$$

where i is the current density at respectively the high and low methanol concentration, c, of each region (so 3.0 and 1.5 M, or 1.5 and 0.75 M). Now equations to calculate an estimate current density (i_{est}) for any inlet feed concentration (c_{inlet}) in each of the two regions can be obtained:

$$i_{est} = m \cdot (c_{inlet} - c_{0.75M}) + i_{0.75M} \quad 75 < [MeOH] < 1.5 \tag{2a}$$

$$i_{est} = m \cdot (c_{inlet} - c_{1.5M}) + i_{1.5M} \quad 1.5 < [MeOH] < 3.0 \tag{2b}$$

Using the calculated values for i_{est}, the outlet concentration (c_{outlet}) for an individual cell can be calculated using:

$$c_{outlet} = c_{inlet} - \frac{6 \cdot i_{est}}{F \cdot Q} \tag{3}$$

where F is Faraday's constant, and Q is the volumetric flow rate of the methanol stream.

These aforementioned equations were used in a repetitive fashion to simulate several electrodes in series until c_{outlet}, was 0.75 M, which corresponds to a conversion of 75%. Specifically, in the empirical model, the inlet methanol concentration, c_{inlet}, for the first electrode was 3 M. The current from the first electrode, i_{act}, was estimated based on calculations using Eqs. (1) and (2). The outlet concentration, c_{outlet}, for the first electrode was calculated using Eq. (3). This process was repeated for additional electrodes with the inlet concentrations for the subsequent electrodes being defined by

the outlet concentration of the previous electrode. Once the final outlet concentration, c_{outlet}, was below 0.75 M, the total electrode surface area was calculated by multiplying the number of electrodes required for the given conversion with the surface area of the given electrode (e.g., 16 electrodes × 1.08 cm^2 per electrode=17.3 cm^2).

3. Results and discussion

3.1. Influence of electrode length on performance

The influence of electrode length on power and current output was investigated by changing the exposed electrode length (2.25, 4.5, 9, and 18 mm) of both the anode and cathode in a direct methanol LFFC (Fig. 1). Peak power outputs of 7.5, 4.3, 3.1, and 1.7 mW at current outputs of 24, 19.2, 14.4, and 8.1 mA were observed for 18, 9, 4.5, and 2.25-mm length electrodes, respectively (Fig. 2(a)). These results corresponded to peak power, and max current densities of 13.9, 16.1, 23.1, and 24.9 mW cm^{-2} and 45, 71, 107, and 121 mA cm^{-2}, respectively for 18, 9, 4.5, 2.25-mm length electrodes (Fig. 2(b)). While the power output consistently drops with electrode length, the first eighth (2.25 mm) and quarter (4.5 mm) of the electrode produces 23% and 41% of the total power output obtained when using the full 18-mm electrode length, respectively. Both the maximum current and power densities at electrode lengths of 4.5 and 2.25 mm are similar to or better than the current and power densities typically observed for Nafion-based DMFCs and miniaturized conventional DMFCs (100–150 mA cm^{-2} and 15–20 mW cm^{-2}, respectively [2,38–41]).

Fig. 2(c) shows the individual electrode polarization plots for the aforementioned experiments. In general, both anode and cathode performance per unit area improved with decreasing electrode length due to the reduced boundary layer effects. The 2.25- and 4.5-mm length anodes had later onsets of mass transport losses, around 150 mA cm^{-2}, as compared to the 18- and 9-mm length anodes, which had onsets of mass transport losses in the range of 50–75 mA cm^{-2} (Fig. 2(c)). However, little difference was observed between the 4.5- and 2.25-mm length anodes. This observation suggests that other factors may dominate in the first 4.5 mm of the electrode length. Specifically, catalyst roughness, typically on the order of 10–30 μm [42], may hinder diffusion more than boundary layer depletion for the first 4.5 mm, given that the boundary layer thickness is on the order of 15 μm [31]. The roughness within the catalyst layer may explain why the power density curves for 4.5- and 2.25-mm lengths anodes are similar, whereas simulations predict significantly higher power density curves for even shorter electrodes [28,31].

3.2. Optimal aspect ratio for a single electrode

The experiments presented above show that shortening electrode length leads to higher power densities, but the absolute amount of power generated is reduced, as expected (Fig. 2(a)). This result suggests that using wider electrodes will be beneficial to achieve both higher power densities as well as higher absolute power. Changing the electrode aspect ratio (i.e., by widening the flow channel), while keeping the total electrode area and the volumetric flow rate constant, affects the development of the boundary layer in two ways: (1) The lower linear velocity increases the boundary layer thickness at the end of the electrode; and (2) shorter electrodes result in a less developed (thinner) boundary layer.

To systematically study the influence of electrode aspect ratio, as defined as the ratio of the electrode length-to-width, on both current and power output, we relied on geometric and dynamic
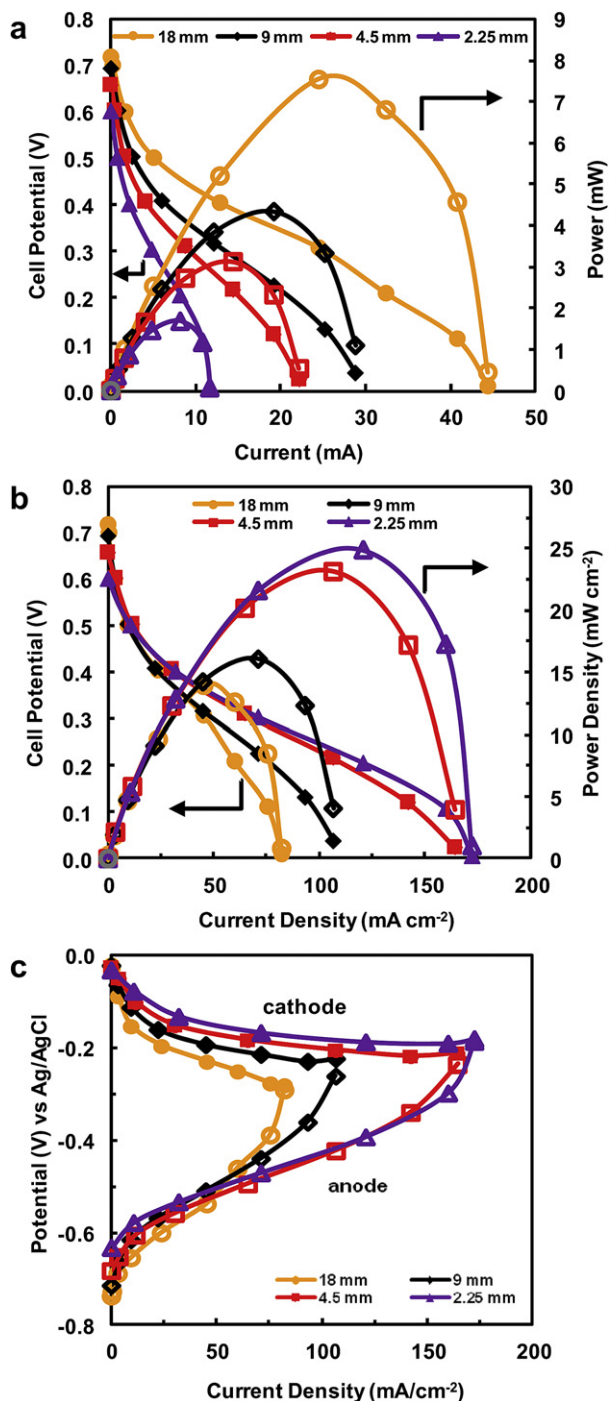
Fig. 2. (a) Polarization and power curves of an air-breathing LFFC for electrode lengths 18, 9, 4.5, and 2.25 mm. (b) Corresponding polarization and power density curves and (c) anode and cathode polarization curves normalized to the electrode area. In all experiments were performed with [MeOH] = 2 M, [KOH] = 1 M, and a flow rate for each stream of 0.1 ml min^{-1}.

simulated (0.15 ml min^{-1}) was achieved by flowing the fuel streams at 0.2, 0.1, and 0.05 ml min^{-1} in the actual experiments performed in cells with 18, 9, and 4.5 mm electrodes, respectively (Fig. 3(a)), and thus making these experimental conditions equivalent to the conditions we are actually interested in. The flow channel width was assumed to have a minimal influence on performance because the flow profile is primarily affected by the distance between electrodes, which is the critical dimension for the development of the flow profiles, which allowed us to use a fixed-width channel of 3 mm to simulate electrodes with three different widths.

Fig. 3(b) shows the normalized cell performance for electrode lengths of 18, 9, and 4.5 mm operated at 0.2, 0.1, and 0.05 ml min^{-1} to simulate electrode areas of 4.5×9 mm^2 (1:2), 9×4.5 mm^2 (2:1), and 18×2.25 mm^2 (4:1). Maximum power densities of 24, 15, and 14 mW cm^{-2} at current densities of 120, 64, and 54 mA cm^{-2} were observed for simulated electrode areas of 4.5×9 mm^2, 9×4.5 mm^2, and 18×2.25 mm^2, respectively. The shorter and wider aspect ratios exhibit much higher current densities and fuel conversion for a given flow rate and electrode area. Specifically, the electrode performance increased by 70% with the low aspect ratio (1:2) configuration compared to a high aspect ratio (4:1)
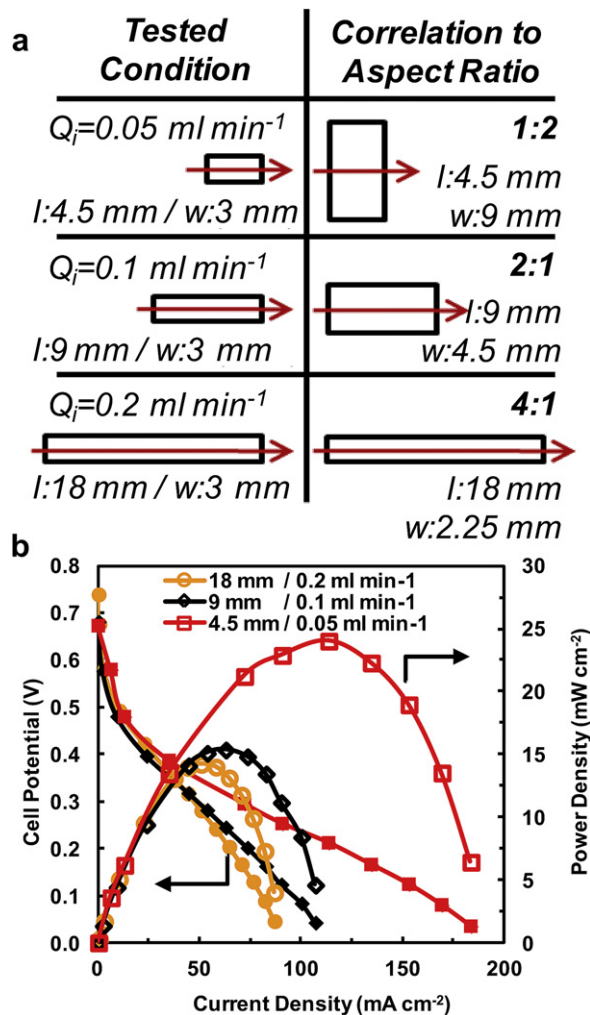

Fig. 3. (a) Schematic of the conditions tested and their correlation to simulated scenarios. (b) Polarization and power density curves of an air-breathing LFFC for electrode lengths 18, 9, and 4.5 mm operated at fuel and electrolyte flow rates of 0.2, 0.1, and 0.05 ml min^{-1}, respectively. In all experiments, [MeOH] = 0.75 M and [KOH] = 1 M.

similarities between the aforementioned LFFC and various aspect ratio electrodes and to empirically model electrodes of various aspect ratios via experimental data with the aforementioned LFFC. So, rather than building several new cell designs, we equipped this LFFC with 4.5, 9, and 18 mm electrodes to experimentally simulate electrode aspect ratios of 1:2 (4.5×9 mm^2), 2:1 (9×4.5 mm^2), and 4:1 (18×2.25 mm^2). The electrode surface area is identical for these three cases (0.4 cm^2). The flow rate of the electrodes

configuration. Most microfluidic LFFCs reported in the literature [5] use electrodes with high aspect ratios (long and narrow) as they easily develop uniform flow fields and facilitate high fuel conversion at reasonable flow velocities. Our data suggests that a low aspect ratio (short and wide) would significantly improve the performance of a single electrode LFFC. The results obtained here, which show that shorter and wider electrodes will improve the performance of an air-breathing alkaline fuel cell configuration, will be applicable to the design of other single cell microfluidic systems for electrochemical processes, not just fuel cells, with different arrangements and reactants.

3.3. Optimal electrode length for multichannel configurations

Above, we reported how to optimize the performance of a single electrode configuration. Scaling to achieve the power output needed for specific applications will require the creation of multichannel configurations. Through a combined simulation and experimental approach, we study how to optimize fuel conversion when using different multi-electrode arrangements.

To model conversion for a series of electrodes, the current density across a single electrode was measured for various methanol concentrations (0.75, 1.5, and 3.0 M), flow rates (0.0125, 0.025, 0.05, 0.1, 0.2, 0.4, and 0.8 ml min^{-1}), and electrode lengths (9, 18, and 36 mm) at the potential which corresponds to peak power (0.2 V). The main effects and interaction plots may be found in the Supplementary information. Interpolation of the experimental data over the concentration range of 0.75–1.5 M and 1.5–3.0 M, as explained in Section 2.4 of the experimental, we can estimate the current for any inlet concentration (Eqs. (2a) and (2b)), and by using the estimated current, we can calculate the outlet concentration (Eq. (3)). Next, we used the outlet concentration of the first electrode as the inlet concentration of the second to calculate (again with Eqs. (2) and (3)) the outlet concentration of the second electrode, and so on, until the outlet concentration is only 25% of the original inlet concentration. So for each of the three electrode lengths, we determined the number of them needed to accomplish a conversion of 75%. By adding the area of the electrodes required for the specified conversion, the total electrode area needed was calculated for each electrode length and flow rate tested (Table 1).

A decrease in the electrode length necessitates more electrodes to accomplish the aforementioned 75% conversion. However, as Table 1 shows, the corresponding total electrode surface area decreases. This decrease in normalized electrode area is more pronounced at slower flow rates. Specifically, at a flow rate of 0.0125 ml min^{-1}, the necessary electrode area for 75% conversion was reduced by 61% (3.5 vs. 8.6 cm^2) by using thirteen 9-mm electrodes as compared to eight 36-mm electrodes. In contrast, at a flow rate of 0.8 ml min^{-1}, the necessary electrode area was only reduced 18% (187.4 vs. 229.0 cm^2) by using 694 9-mm electrodes as compared to 212 36-mm electrodes.

Next, we wished to compare these datasets with respect to surface reaction rates to better enable comparison of the total electrode areas needed to accomplish 75% conversion at different flow rates. Fig. 4 shows methanol reaction rates normalized to the total electrode surface area (in mmol min^{-1} mm^2) for a 3.0 M methanol fuel stream converted across a series of electrodes (each 9, 18, or 36-mm long) to 0.75 M (75% conversion) for each flow rate tested.

While the shorter electrodes universally improve the normalized reaction rates, the improvement is more pronounced for slower flow rates because the boundary layer becomes thicker. Specifically, at a flow rate of 0.0125 ml min^{-1}, the resultant normalized reaction rate for 75% conversion increases by 146% (1.07 vs. 0.43 mmol min^{-1} mm^2) by using 9-mm electrodes instead of 36-mm electrodes. In contrast, at a higher flow rate of 0.8 ml min^{-1}, the necessary electrode area only increases by 22% (1.28 vs. 1.05 mmol min^{-1} mm^2) by using 9-mm electrodes instead of 36-mm electrodes.

The more pronounced influence of electrode length on conversion at slow flow rates stems from an increase in reactant depletion due to slower fuel flow rates. This effect can be explained by applying the Blasius solution for boundary layer thickness (Eq. (4)):

$$\delta \approx 5 \sqrt{\frac{\nu x}{u_0}} \tag{4}$$

where δ. the boundary layer thickness as defined by the point where the fluid velocity has come within 1% of the 'free stream' velocity, u_0, ν is the kinematic viscosity, and x is the distance down the electrode [40]. This equation shows that the boundary layer becomes thicker upon decreasing the flow rate. As a result, the cell becomes diffusion limited at slower flow rates, a limitation that can be overcome by using many short electrodes.

The results here show that using several "short" electrodes in series results in much higher conversion normalized to the surface area than fewer "longer" electrodes, especially at slow flow rates. Consequently, applications that require low power for long periods of time, for which fuel utilization is important, would benefit from stack designs with multiple electrodes. In contrast, applications requiring large amounts of power for short periods of time need to operate at higher flow rates and do not benefit as much from series of short electrodes.

One practical aspect that we did not discuss above is the need to homogenize the fuel concentration in the fuel stream before it enters the inlet of the next cell, after emerging from the outlet of the previous cell with a depleted boundary layer. In the simulations
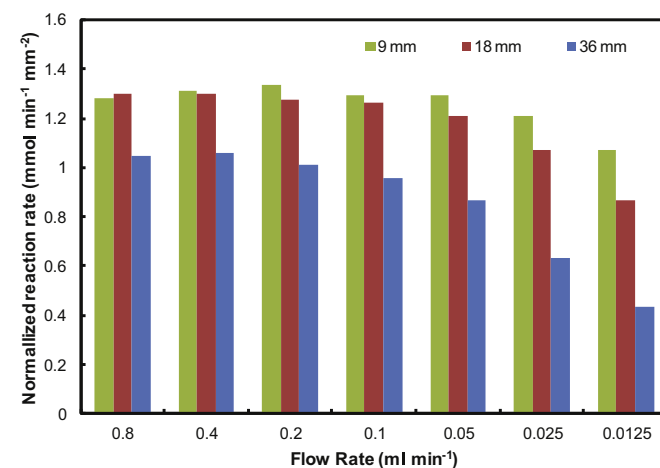
Table 1
Absolute electrode area (cm^2) required for a multiple electrode arrangement for 75% conversion of a methanol fuel stream.

Electrode length (mm)	Flow rate (ml min^{-1})						
	0.8	0.4	0.2	0.1	0.05	0.025	0.0125
36	228.96	113.4	59.4	31.32	17.28	11.88	8.64
18	184.68	92.34	46.98	23.76	12.42	7.02	4.32
9	187.38	91.53	44.82	23.22	11.61	6.21	3.51

Fig. 4. Reaction rate of methanol within the fuel stack relative to the total electrode area, predicted based on a model for the use of a fuel cell stack for the conversion of methanol from 3.0 M to 0.75 M with variable length electrodes (9, 18, and 36 mm) in a stack arrangement.

above, we assumed that a stream of uniform, but lower, fuel concentration would enter each successive cell. To homogenize the fuel stream between successive cells, one could use one of many microfluidic mixing methods, *e.g.*, a herringbone mixer [28,43] or multiple inlets (or outlets) along a single electrode to periodically push away (or remove) the depleted boundary layer [30]. However, the addition of mixers or multiple inlets (outlets) adds complexity to the system and reduces spatial density of the stack. Consequently, an optimal design for a given application will need to balance the desire to minimize electrode length with the need for homogenization of the fuel stream between successive cells, which adds additional volume and complexity to the stack.

4. Conclusions

Here, we studied the influence of boundary layer depletion on performance in an alkaline, air-breathing LFFC as a function of electrode length, electrode arrangement, and flow rate. Both the current and power densities obtained here for LFFCs are similar to or better than Nafion-based DMFCs and miniaturized conventional DMFCs [2,38–41]. We confirmed that higher current densities can be achieved when using shorter electrodes. The power density increased, respectively, by 65 and 88% for 4.5-mm and 2.25-mm long electrodes compared to an 18-mm electrode. While shorter electrodes lead to higher current densities, the absolute current decreases, suggesting that arranged multiple short electrodes in series can improve overall performance.

To utilize the increased power densities from shorter electrodes, we explored different electrode arrangements and aspect ratios. Shorter and wider electrodes exhibit notably higher current densities and conversions for a given flow rate and electrode area. Specifically, a 67% increase in performance was observed when switching to a 1:2 aspect ratio (length-to-width) from a 4:1 aspect ratio. So by changing the standard operating aspect ratio, the performance of single channel electrodes can be improved significantly.

Alternatively, the use of shorter electrodes in series will allow for higher fuel conversion while maintaining higher current densities. We observed that the improvement in reaction rate normalized by surface area as a result of shortening the electrode length is much more pronounced when operating at slow flow rates. Consequently, arrangements comprised of shorter electrodes will be most suitable for applications that require low power for long periods of time, for which fuel utilization is important. However, in arrangements comprised of multiple electrodes, the fuel stream (with depleted boundary layer) must be homogenized between consecutive cells, which will add additional volume to a stack. The analysis reported here for LFFCs can also be applied in the development and optimization of other microfluidic electrochemical reactor designs [44–46].

Appendix A. Supplementary data

Supplementary data associated with this article can be found, in the online version, at http://dx.doi.org/10.1016/j.jpowsour.2012.06.061.

References

[1] L. Carrette, K.A. Friedrich, U. Stimming, ChemPhysChem 1 (2001) 5–39.
[2] A. Kundu, J.H. Jang, J.H. Gil, C.R. Jung, H.R. Lee, S.H. Kim, B. Ku, Y.S. Oh, Journal of Power Sources 170 (2007) 67–78.
[3] S. Pennathur, J.C.T. Eijkel, A. Van Den Berg, Lab on a Chip – Miniaturisation for Chemistry and Biology 7 (2007) 1234–1237.
[4] C.K. Dyer, Journal of Power Sources 106 (2002) 31–34.
[5] E. Kjeang, N. Djilali, D. Sinton, Journal of Power Sources 186 (2009) 353–369.
[6] C. Potera, Environmental Health Perspectives 115 (2007) A38–A41.
[7] P.O. López-Montesinos, N. Yossakda, A. Schmidt, F.R. Brushett, W.E. Pelton, P.J.A. Kenis, Journal of Power Sources 196 (2011) 4638–4645.
[8] N.T. Nguyen, S.H. Chan, Journal of Micromechanics and Microengineering 16 (2006) R1–R12.
[9] A.V. Tripkovic, K.D. Popovic, B.N. Grgur, B. Blizanac, P.N. Ross, N.M. Markovic, Electrochimica Acta 47 (2002) 3707–3714.
[10] K.F. Blurton, E. McMullin, Energy Conversion 9 (1969) 141–144.
[11] J.R. Varcoe, R.C.T. Slade, Fuel Cells 5 (2005) 187–200.
[12] M. Schulze, E. Gülzow, Journal of Power Sources 127 (2004) 252–263.
[13] N. Wagner, M. Schulze, E. Gülzow, Journal of Power Sources 127 (2004) 264–272.
[14] F.R. Brushett, M.S. Thorum, N.S. Lioutas, M.S. Naughton, C. Tornow, H.-R.M. Jhong, A.A. Gewirth, P.J.A. Kenis, Journal of the American Chemical Society 132 (2010) 12185–12187.
[15] C. Coutanceau, L. Demarconnay, C. Lamy, J.M. Léger, Journal of Power Sources 156 (2006) 14–19.
[16] E.R. Choban, L.J. Markoski, A. Wieckowski, P.J.A. Kenis, Journal of Power Sources 128 (2004) 54–60.
[17] E. Kjeang, R. Michel, D.A. Harrington, D. Sinton, N. Djilali, Electrochimica Acta 54 (2008) 698–705.
[18] R.S. Jayashree, S.K. Yoon, F.R. Brushett, P.O. Lopez-Montesinos, D. Natarajan, L.J. Markoski, P.J.A. Kenis, Journal of Power Sources 195 (2010) 3569–3578.
[19] J. Xuan, M.K.H. Leung, D.Y.C. Leung, M. Ni, H. Wang, International Journal of Hydrogen Energy 36 (2011) 11075–11084.
[20] E. Kjeang, R. Michel, D.A. Harrington, N. Djilali, D. Sinton, Journal of the American Chemical Society 130 (2008) 4000–4006.
[21] W. Sung, J.W. Choi, Journal of Power Sources 172 (2007) 198–208.
[22] E. Kjeang, J. McKechnie, D. Sinton, N. Djilali, Journal of Power Sources 168 (2007) 379–390.
[23] K.S. Salloum, J.R. Hayes, C.A. Friesen, J.D. Posner, Journal of Power Sources 180 (2008) 243–252.
[24] K.S. Salloum, J.D. Posner, Journal of Power Sources 196 (2011) 1229–1234.
[25] J.L. Cohen, D.A. Westly, A. Pechenik, H.D. Abruna, Journal of Power Sources 139 (2005) 96–105.
[26] A. Li, S.H. Chan, N.T. Nguyen, Journal of Micromechanics and Microengineering 17 (2007) 1107–1113.
[27] M.H. Chang, F. Chen, N.S. Fang, Journal of Power Sources 159 (2006) 810–816.
[28] S.K. Yoon, G.W. Fichtl, P.J.A. Kenis, Lab on a Chip 6 (2006) 1516–1524.
[29] J. Xuan, D.Y.C. Leung, M.K.H. Leung, H. Wang, M. Ni, Journal of Power Sources 196 (2011) 9391–9397.
[30] A.S. Hollinger, R.J. Maloney, R.S. Jayashree, D. Natarajan, L.J. Markoski, P.J.A. Kenis, Journal of Power Sources 195 (2010) 3523–3528.
[31] A. Bazylak, D. Sinton, N. Djilali, Journal of Power Sources 143 (2005) 57–66.
[32] A. Ebrahimi Khabbazi, A.J. Richards, M. Hoorfar, Journal of Power Sources 195 (2010) 8141–8151.
[33] R.S. Jayashree, L. Gancs, E.R. Choban, A. Primak, D. Natarajan, L.J. Markoski, P.J.A. Kenis, Journal of the American Chemical Society 127 (2005) 16758–16759.
[34] D.P. Davies, P.L. Adcock, M. Turpin, S.J. Rowen, Journal of Power Sources 86 (2000) 237–242.
[35] F.R. Brushett, W.P. Zhou, R.S. Jayashree, P.J.A. Kenis, Journal of the Electrochemical Society 156 (2009) B565–B571.
[36] M.S. Naughton, F.R. Brushett, P.J.A. Kenis, Journal of Power Sources 196 (2011) 1762–1768.
[37] E.R. Choban, P. Waszczuk, P.J.A. Kenis, Electrochemical and Solid-State Letters 8 (2005) A348–A352.
[38] S.C. Kelley, G.A. Deluga, W.H. Smyrl, Electrochemical and Solid-State Letters 3 (2000) 407–409.
[39] T. Shimizu, T. Momma, M. Mohamedi, T. Osaka, S. Sarangapani, Journal of Power Sources 137 (2004) 277–283.
[40] T.J. Yen, N. Fang, X. Zhang, G.Q. Lu, C.Y. Wang, Applied Physics Letters 83 (2003) 4056–4058.
[41] V. Baglio, A. Stassi, E. Modica, V. Antonucci, A.S. Aricò, P. Caracino, O. Ballabio, M. Colombo, E. Kopnin, Electrochimica Acta 55 (2010) 6022–6027.
[42] A. Bauer, E.L. Gyenge, C.W. Oloman, Electrochimica Acta 51 (2006) 5356–5364.
[43] A.D. Stroock, S.K.W. Dertinger, A. Ajdari, I. Mezic, H.A. Stone, G.M. Whitesides, Science 295 (2002) 647–651.
[44] D.T. Whipple, E.C. Finke, P.J.A. Kenis, Electrochemical and Solid-State Letters 13 (2010) D109–D111.
[45] D.T. Whipple, P.J.A. Kenis, Journal of Physical Chemistry Letters 1 (2010) 3451–3458.
[46] B.A. Rosen, A. Salehi-Khojin, M.R. Thorson, W. Zhu, D.T. Whipple, P.J.A. Kenis, R.I. Masel, Science 334 (2011) 643–644.